Journal of Electron Spectroscopy and Related Phenomena 195 (2014) 48–54

Contents lists available at ScienceDirect

Journal of Electron Spectroscopy and Related Phenomena

journal homepage: www.elsevier.com/locate/elspec

High resolution electron spectrometers for characterizing the contrast of isolated 25 as pulses

Qi Zhang, Kun Zhao, Zenghu Chang*

Institute for the Frontier of Attosecond Science and Technology, CREOL and Department of Physics, University of Central Florida, Orlando, FL 32816, USA

ARTICLE INFO

Article history:
Received 13 January 2014
Received in revised form 17 March 2014
Accepted 8 May 2014
Available online 24 May 2014

Keywords:
Magnetic bottle electron energy spectrometer
Isolated attosecond pulse characterization
High-order harmonic generation
X-ray source
Ultrafast laser source

ABSTRACT

We quantify the effects of the energy resolution of a magnetic bottle electron spectrometer in an attosecond streak camera on the accuracy of measuring the relative amplitudes of satellite pulses around the main attosecond pulse. Our numerical simulations show that the spectral resolution can be significantly improved by restricting the acceptance angle using a pinhole located near the source of the photoelectrons. The intensity of the pre- and post-pulses which are 1% and 10% of a main 25 as pulse can potentially be measured with less than 10% error by two practical time-of-flight spectrometer designs.

© 2014 Elsevier B.V. All rights reserved.

1. Introduction

When an isolated attosecond light pulse is generated from a gas medium driven by an intense femtosecond laser, the main pulse is always accompanied by pre- and post-pulses, usually referred to as satellite pulses, regardless of the gating technique used [1–3]. Since attosecond pump-attosecond probe experiments for studying electron dynamics require minimum disturbance of the system before and after the main pulse, the intensity of the satellite pulses should be 10% or less of the primary pulse. The contrast of the attosecond extreme ultraviolet (XUV) pulses can be retrieved from attosecond streaking traces [4]. Previously, experimental defects that affect the satellite pulse retrieval have been discussed for pulses longer than 80 as in [5–9]. However, the effect of the spectrometer resolution, which is of critical importance for characterizing a broadband XUV pulse, has not been discussed in detail. In this report, we studied the effects of the energy resolution of the electron spectrometer on the accurate characterization of the pre- and post-pulses surrounding a 25 as main pulse, which corresponds to one atomic unit of time. Briefly, the current experimental setup is discussed in Section 2. The resolution of the spectrometer is numerically evaluated in Section 3. Two methods to improve the energy resolution are discussed in Section 4 and the performance on satellite pulse retrieval of the new designs is shown in Section 5.

2. Current setup

We consider an attosecond streak camera based on a magnetic bottle electron spectrometer (MBES) as shown in Fig. 1, with which 67 as pulses were recently demonstrated [10]. This type of time-of-flight (TOF) spectrometer is chosen because of its high collection efficiency and high energy resolution [11–13]. The details of the spectrometer have been described elsewhere [14]. Briefly, a rare earth magnet (NdFeB) and a conical pole piece made of soft iron create a 0.8 Tesla magnetic field at the surface of the pole piece. A gas jet with 50 μm inner diameter is located 1 mm away from the tip of the pole piece, where the XUV pulse is focused to produce photoelectrons from the target atoms. A solenoid coil is wrapped around the 3 m long flight tube to generate 10 Gauss magnetic field, and a microchannel plate (MCP) detector is mounted at the end of the flight tube to record the photoelectron signal. The photoelectrons enter the fight tube through an aperture with a diameter D, which was designed for differential pumping. The diameter of the aperture is 1 mm, much large than the electron beam diameter there. Fig. 1(b) shows the enlarged diagram of the magnet and aperture with the photoelectron angular distribution.

3. MBES resolution and satellite pulse retrieval

To evaluate the energy resolution of the MBES, the electron trajectories and their flight times are traced by numerical simulations [15]. As shown in Fig. 2(a) for a monoenergetic source of 180 eV electrons, the energy calculated from the flight time depends on

* Corresponding author. Tel.: +1 4078234442.
E-mail address: Zenghu.Chang@ucf.edu (Z. Chang).

http://dx.doi.org/10.1016/j.elspec.2014.05.008
0368-2048/© 2014 Elsevier B.V. All rights reserved.

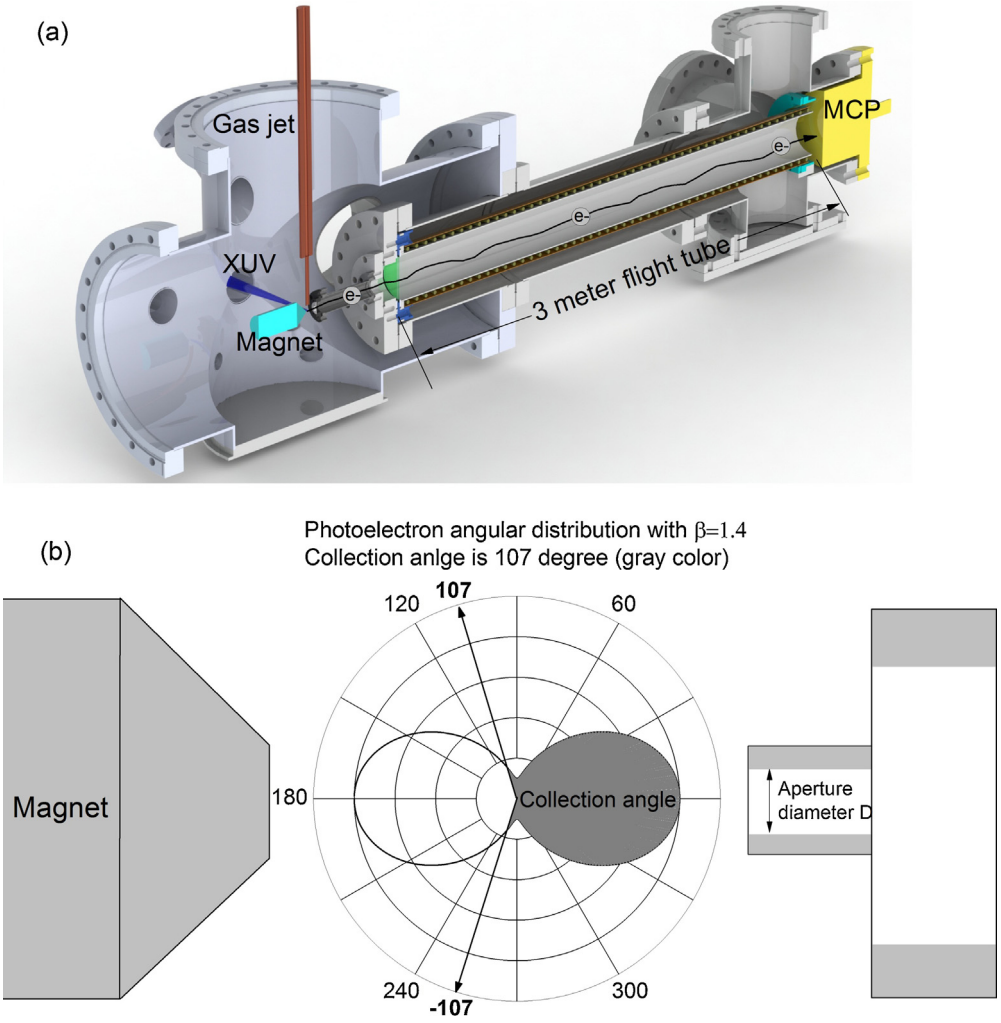

Fig. 1. (a) Diagram of magnetic bottle electron spectrometer (MBES) with a 3 m long flight tube. The XUV beam is focused at 1 mm away from the magnet which produces a highly diverging magnetic field and a 50 μm diameter stainless steel gas jet is placed on top of the XUV beam. Photoelectrons enter an aperture with a diameter D and fly through the 3 m long tube before reaching the MCP detector. A solenoid coil with 0.8 A current is wrapped around the flight tube to supply a 10 Gauss magnetic field. A μ-metal tube is placed outside the flight tube to shield the earth magnetic field. (b) An enlarged schematic diagram of the magnet and aperture. The plot in polar coordinates shows the photoelectron angular distribution with an asymmetry of 1.4. The collection angle of the MBES is calculated to be 107°. The solid angle within which the photoelectrons can be collected by the MBES is shown in gray color.

the emission angle of the photoelectron relative to the axis of the flight tube. This energy should be regarded as the "TOF energy", which is different from the true initial kinetic energy of the photoelectrons. The larger the emission angle, the more the TOF energy deviates from the true value. For electrons emitted at 107°, which is the largest accepting angle of the current setup as shown in Fig. 1(b), the difference between the two values reaches 1.8% for a 3 m long TOF.

The angular distribution of the photoelectrons from a given target atom is given by:

$$\frac{d\sigma}{d\Omega} \propto 1 + \frac{\beta}{2}[3\cos^2(\theta) - 1], \quad (1)$$

where $d\sigma/d\Omega$ is the differential photoionization cross section, θ is the emission angle, and β is the asymmetry [16]. Neon is used in the simulations due to its large photoionization cross section and nearly constant β value for energies above 40 eV [16]. Using the above equation and the results shown in Fig. 2(a), we plot in Fig. 2(b) the TOF energy distribution of monoenergetic 180 eV electrons with all possible emission angles, which is referred to as the "response function" of the MBES. The long tail in the low energy part of the response function results from electrons with large emission angles. We note that with this unique distribution, it is not appropriate to define the energy resolution by the full-width-at-half-maximum (FWHM) because it does not reflect the contribution of the long tail.

To study the effect of the MBES resolution on the satellite pulse retrieval, we use a 25 as transform-limited (TL) Gaussian pulse, with central photon energy at 151 eV. It has pre- and post-pulses with 1% intensity contrast to the main pulse. The satellite pulses have 50 as pulse duration with the same central photon energy and are ±2500 as away from the main pulse, as depicted in Fig. 3(a). The spacing equals to one optical period of the driving laser centered at 750 nm, which is typical for the Double Optical Gating [3]. The corresponding photoelectron spectrum is shown with black solid line in Fig. 3(b), which spans from 30 to 220 eV.

The red dashed line in Fig. 3(b) represents the energy spectrum after convoluting the real spectrum with the MBES response function calculated with the 3 m flight tube. The response function was normalized to its area before the convolution to ensure the equal weight for all energies. A streaking spectrogram is then generated numerically with the XUV pulse and a 5 fs, 750 nm near infrared (NIR) streaking pulse which has a peak intensity of 5×10^{11} W/cm^2. The spectrum in each delay in the streaking

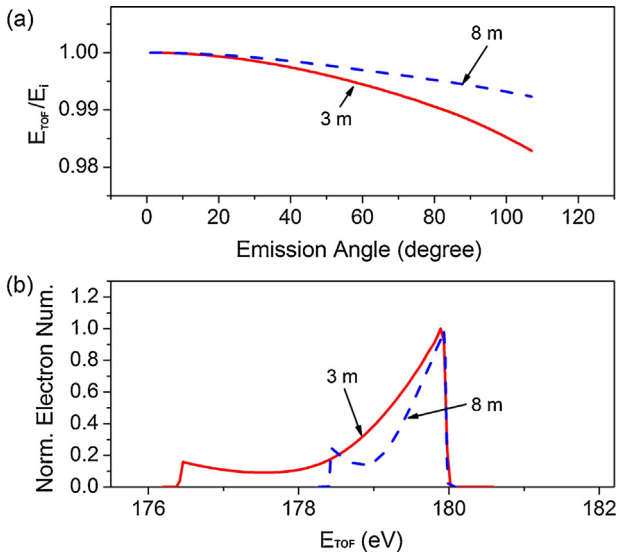

Fig. 2. (a) Ratio of the energy calculated from the flight time (E_{TOF}) to the real value (E_i) as a function of the emission angle. Electrons with emission angles larger than 107° cannot be detected by the MCP. (b) Energy distribution of 180 eV monoenergetic electrons calculated assuming the angular distribution of Ne photoionization with an asymmetry of 1.4, which is referred to as the response function. The solid line is for a spectrometer with 3 m flight distance; and the dashed line is for an 8 m TOF calculated for Section 4.

spectrogram is also convoluted with the response function, as shown in Fig. 3(c). The FROG-CRAB technique [4] is used to reconstruct the spectrogram, as shown in Fig. 3(d). The retrieved temporal intensity profile is plotted in Fig. 3(a), as a comparison with the input pulse. The result retrieved from such a streaking trace indicates that the satellite pulses would have a relative intensity of 0.16% of the main pulse, which is much smaller than the real value 1%. The reason is the fringes in the spectrum caused by the interference between the satellite pulses and the main pulse are greatly smeared out by the response function (best seen from the inset of Fig. 3(b)).

Normally the satellite pulse has lower photon energy due to their weaker driving electric field. In this case, the interference pattern will move to lower photoelectron energy range where the spectrometer resolution is better. In addition, for isolated attosecond pulse generated with polarization gating or amplitude gating methods, the satellite pulses are half-cycle away from the main pulse [1,2]. Therefore, the energy difference between two adjacent interference maxima should be twice the maxima separation for double optical gating. In both of these two cases, the contrast measurement with the same MBES resolution would be more accurate than the situation we discuss here. However, in order to keep our discussion more general, we consider the situation which demands the highest resolution, e.g. the satellite pulses have the same central photon energy as the main pulse and are separated from the main pulse by a full laser cycle.

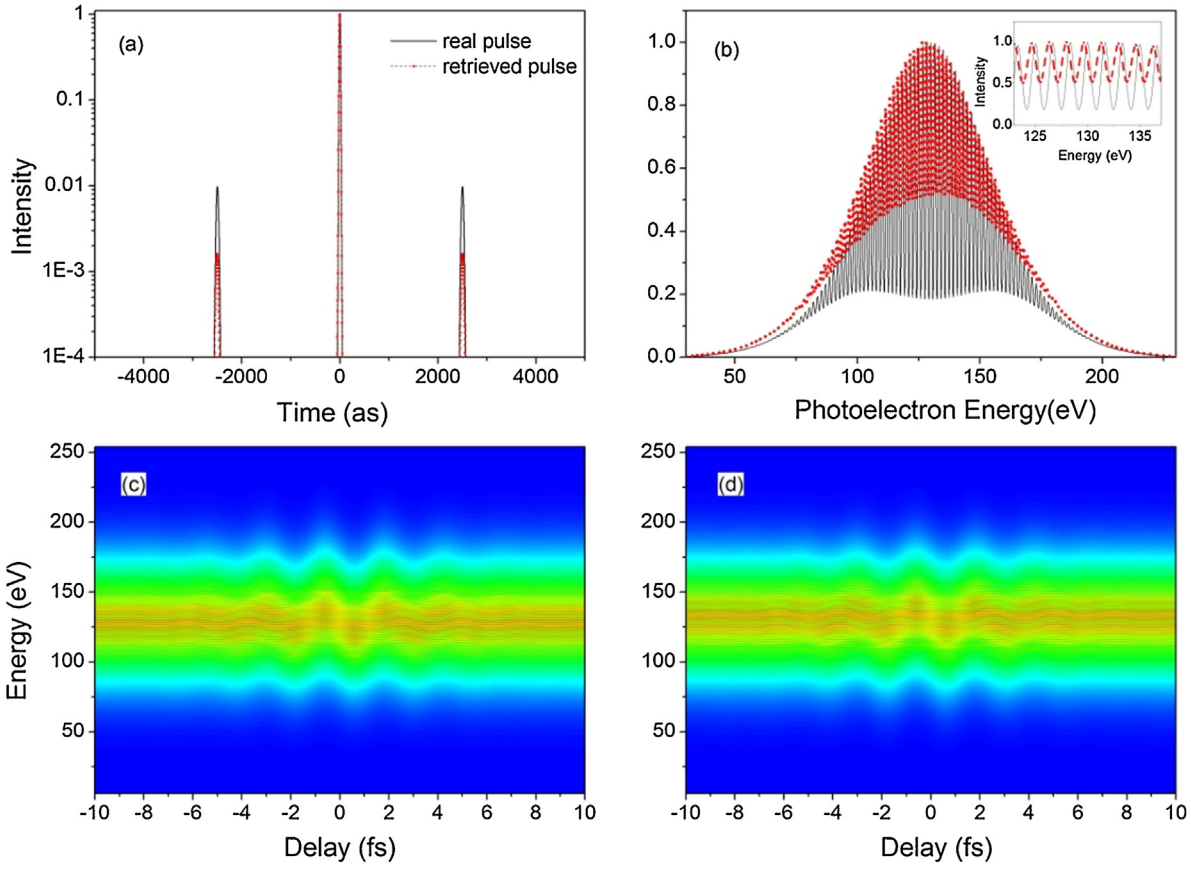

Fig. 3. Effects of the response function on characterizing satellite pulses (1% satellite pulse is assumed). (a) The black solid line shows the input temporal pulse. The red dashed line with dot is the retrieved temporal pulse from the streaking trace in (c). (b) The black solid line shows the spectrum of the input pulse, and the red dashed line is the convoluted spectrum in a 3 m TOF. Inset shows the enlarged spectra from 120 to 140 eV. (c) Streaking spectrogram convoluted with the response function of a 3 m TOF. The streaking NIR pulse has 5 fs pulse duration, with a central wavelength at 750 nm and peak intensity 5×10^{11} W/cm^2. (d) Streaking spectrogram reconstructed by the FROG-CRAB technique after 2000 iterations of the PCGPA algorithm [4,6]. (For interpretation of the references to color in this legend, the reader is referred to the web version of the article.)

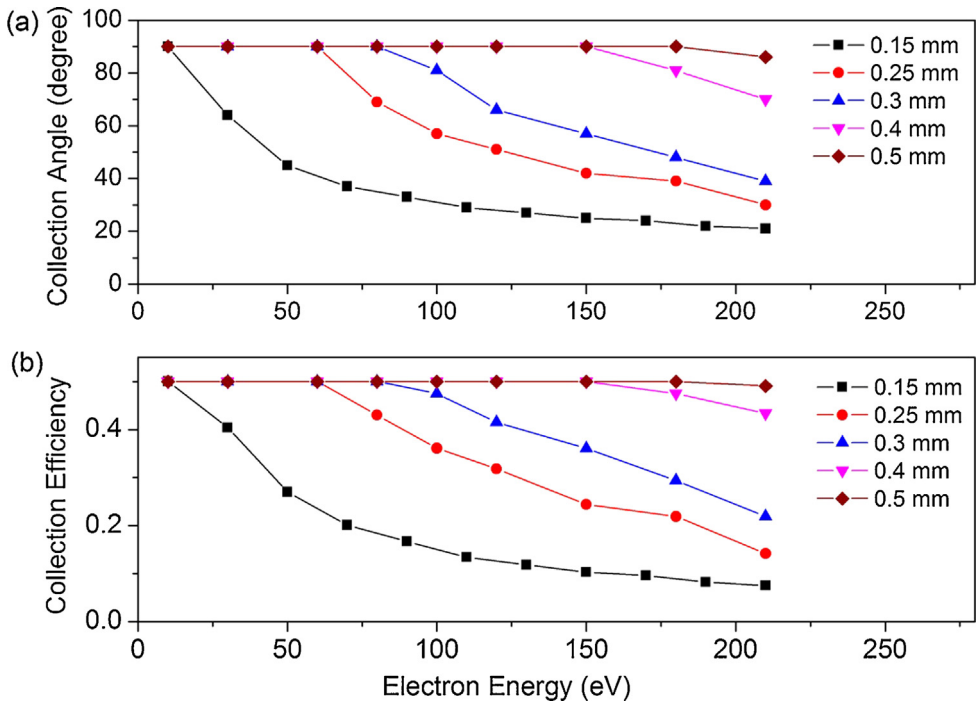

Fig. 4. (a) Collection angle, and (b) collection efficiency as functions of the electron energy for different pinhole diameters.

4. Design for improving resolution

For a given initial energy, the uncertainty in the TOF energy ΔE_{TOF}, is related to the uncertainty in the flight time measurement

$$\frac{\Delta E_{\mathrm{TOF}}}{E_{\mathrm{TOF}}} = 2\frac{\Delta t}{t}, \tag{2}$$

where t is the flight time for an electron emitted along the axis of the flight tube ($\theta = 0$). In most TOF setups, the energy resolution is limited by the detector and data acquisition electronics (DAQ). We have measured our DAQ resolution to be 250 ps [17]. In our case, due to the long flight tube, the intrinsic MBES temporal resolution is usually on the order of 1 ns, which indicate we could neglect the effect of DAQ for most cases in our discussion. However, under certain extreme conditions, such as very large electron energy and very small collection angle, the temporal spread can be small enough so that the DAQ resolution could not be neglected any more. We will discuss the detail when this condition is met later in the paper. In most cases, the temporal spread Δt is mainly caused by off-axis motion of the electrons in the first 100 mm of their trajectories. Therefore, lengthening the flight tube from 3 m to 8 m will increase the flight time t while keeping Δt roughly unchanged, resulting a narrower response function, as shown in Fig. 2(a) and (b). However, even for an 8 m long TOF, the retrieved intensity of the 1% satellite pulses is only 0.37%, which is still much lower than the real value.

Further increasing TOF length will not greatly improve the resolution since the main temporal error will come from the increased flight tube. However, the response function of the MBES can be further narrowed by eliminating electrons with large emission angles. Since large angle electrons deviate transversely away from the axis of the flight tube as they fly in the magnetic field, a pinhole can effectively block them. In principle the pinhole can be placed anywhere between the source and the detector of the photoelectrons; however in experiments it may be easiest to place it near the beginning of the electron trajectory. This effect has been experimentally observed [18]. In our simulations, a pinhole with a diameter D from 0.1 to 0.5 mm is placed 1 mm away from the photoelectron source and 2 mm away from the magnet tip, which replaces the differential pumping aperture shown in Fig. 1.

In Fig. 4(a), the collection angles of electrons for different pinhole sizes are plotted as functions of the electron energy. For each collection angle Θ, there is a corresponding collection efficiency, calculated by:

$$\eta(\Theta) = \frac{\int_0^{\Theta}\left[1+\frac{\beta}{2}(3\ \cos^2(\theta)-1)\right]\sin\ \theta\, d\theta}{\int_0^{\pi}\left[1+\frac{\beta}{2}(3\ \cos^2(\theta)-1)\right]\sin\ \theta\, d\theta}. \tag{3}$$

The dependence of the collection efficiency on the real electron energy is shown in Fig. 4(b). Particularly, the response functions of 180 eV electrons for two cases, 0.15 mm pinhole in 3 m TOF and 0.25 mm pinhole in 8 m TOF, are shown in Fig. 5(a). The long tail is eliminated and the FWHM is only 0.23 eV for the 3 m TOF and 0.19 eV for the 8 m TOF, corresponding to $\Delta E/E \approx 0.13\%$ and 0.11% respectively. We note that, under this extreme condition, the corresponding temporal resolution will become 282 ps for 3 m TOF and 603 ps for 8 m TOF, comparable to the measured DAQ resolution. Thus the total response function will be the convolution of the MBES and DAQ resolution. This convolution will be included in the following simulation.

An important issue for reducing collection angle by this method is that the dependence of the collection efficiency on the electron energy will modify the measured spectrum, hence impact the pulse retrieval. For the 3 m TOF with a 0.15 mm pinhole, Fig. 5(b) shows the comparison between convoluted spectrum with and without this spectral modification caused by the pinhole. Clearly the spectrum is shifted to lower energy due to higher collection efficiency there, and the pulse duration could be changed. To study this effect, the pulse duration before and after the spectral modification are retrieved with different chirps, as shown in Fig. 5(c). For a transform limited pulse, there is no difference in pulse duration. However, as the chirp increases to 5000 as^2, the relative difference of pulse duration caused by this effect reaches 5%.

This modification can be corrected by simply dividing the measured photoelectron spectrum by the corresponding collection

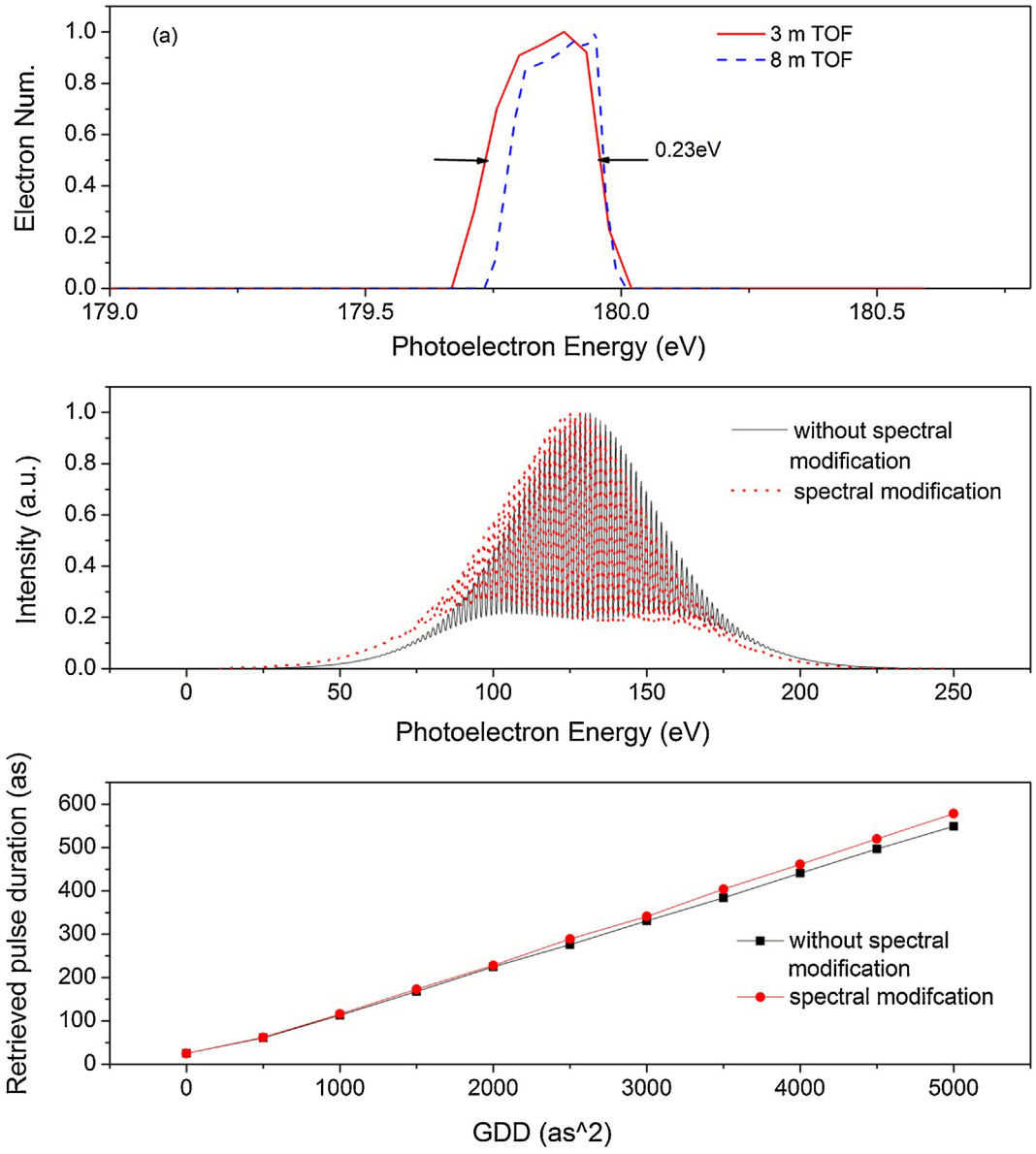

Fig. 5. (a) Response functions calculated with a 0.15 mm diameter pinhole in the 3 m TOF and a 0.25 mm pinhole in the 8 m TOF, for 180 eV electrons. (b) Comparison between convoluted spectra with (red dotted line) and without (black solid line) considering the collection efficiency dependence on photoelectron energy. (c) Comparison of retrieved pulse durations with different chirps with and without considering spectral modification. It shows as the GDD increases to 5000 as^2, the relative difference of the retrieved pulse duration becomes 5%. (For interpretation of the references to color in this legend, the reader is referred to the web version of the article.)

efficiency at each energy. To demonstrate this, we constructed the streaking traces using the spectra in Fig. 5(b) with 5000 as^2 GDD. The streaking traces without and with the spectral correction are plotted in Fig. 6(a) and (b), and the corresponding retrievals are compared with the real pulse in Fig. 6(c) and (d). It can be seen in Fig. 6(c) that the retrieved main pulse is slightly different from the real one due to the spectral shift caused by the pinhole, and can be corrected as shown in Fig. 6(d). The retrieved satellite pulses are not affected by the pinhole (not shown).

5. Performance of the new TOF designs

To reveal the effects of the pinhole size on the accuracy of satellite pulse contrast measurements, we simulated the electron spectra with the response functions calculated for different acceptance angles limited by the pinhole. The retrieved temporal satellite pulse contrasts with different pinhole diameters are plotted in Fig. 7(a) and (b). To compare, the real value is also plotted for satellite pulses with intensities of 1% and 10% of the main pulses. This figure shows that as pinhole size decreases, the satellite pulse characterization becomes more accurate, as expected. Particularly, a 0.25 mm pinhole in an 8 m TOF or a 0.15 mm pinhole in a 3 m TOF can be used to reduce the retrieval error to less than 10%. From Fig. 4(b), the collection efficiency of the 8 m TOF with a 0.25 mm pinhole is higher than 15% in the energy range of 30–220 eV, whereas the efficiency is 50% without the pinhole. The efficiency of the 3 m TOF is about half that for 8 m. This means that the integration time in streaking experiments with the 3 m TOF needs to double that of the 8 m long TOF.

In attosecond streaking experiments, the streaking amplitude decreases as the emission angle increases. Furthermore, electrons emitted with angles larger than 90° will be streaked to the

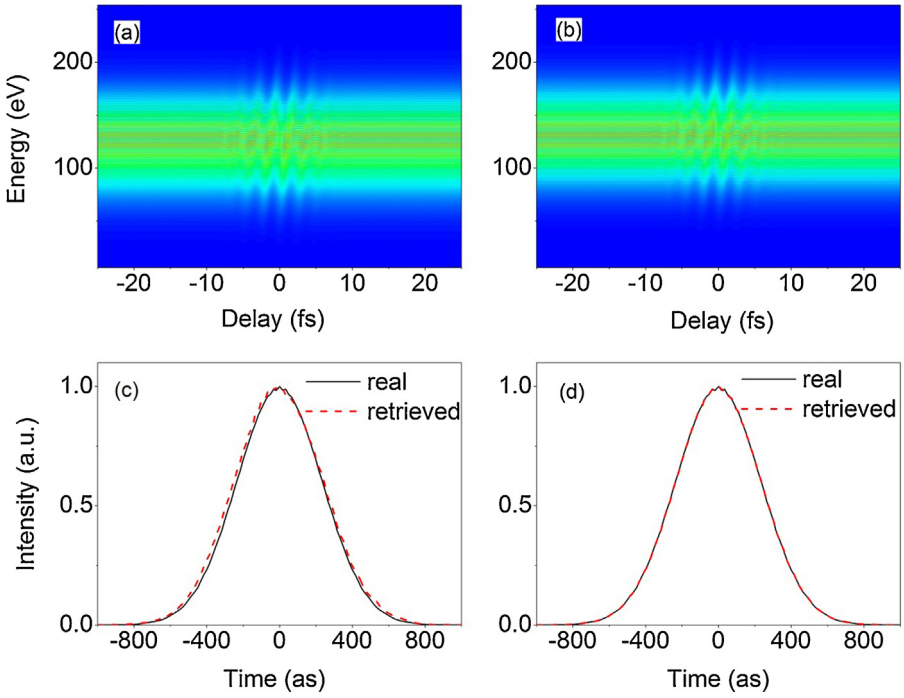

Fig. 6. Effect of collection efficiency dependence on the photoelectron energy to the pulse retrieval. The streaking trace is constructed using the spectra without spectral modification in Fig. 5(b) with a 5000 as^2 GDD. (a) Streaking trace distorted by the energy dependent collection efficiency. (b) Streaking trace corrected by dividing each spectrum by the corresponding collection efficiency. (c) and (d) are retrieved main pulses from (a) and (b) respectively, plotted in red dashed line. Real pulse is plotted as a comparison in (c) and (d) in black solid line. (For interpretation of the references to color in this legend, the reader is referred to the web version of the article.)

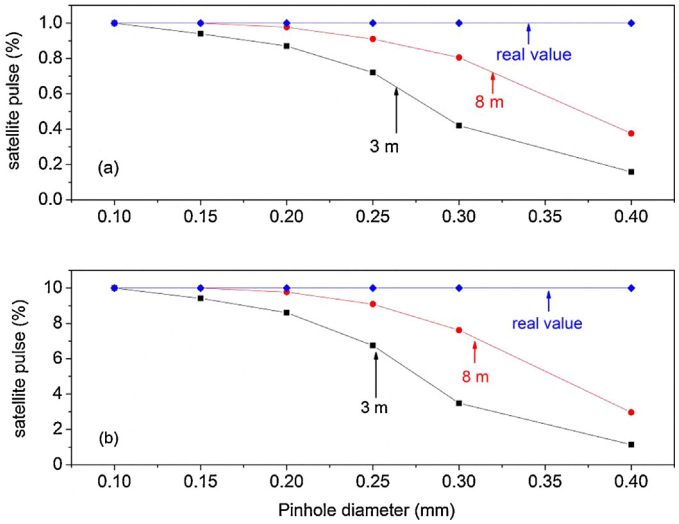

Fig. 7. Comparison of the retrieved satellite pulse contrast limited by MBES resolution with real values. The black line with rectangles shows the retrieved satellite pulse contrast with a 3 m TOF and the red line with circles shows the retrieved contrast with an 8 m TOF. The blue line with diamonds shows the real value of (a) 1% and (b) 10% contrast as a comparison. (For interpretation of the references to color in this legend, the reader is referred to the web version of the article.)

opposite direction. On the other hand, retrieval techniques such as FROG-CRAB and PROOF [4,19] assume the emission angle is zero. Therefore, both the main pulse and the satellite pulses can be retrieved with a better accuracy with the reduced acceptance angle.

6. Conclusions

We have shown that placing a 0.25 mm pinhole near the photoelectron source in an MBES with an 8 m long flight tube, the intensity contrast of satellite pulses to a 25 as main pulse can be potentially measured with less than 10% error. The collection efficiency is 15%, as compared to 50% without the pinhole. Similar accuracy can be reached with a 3 m long TOF when a 0.15 mm pinhole is added, but the collection efficiency is reduced to 7%. One should take into account the laser repetition rate when choosing the MBES design so that a streaking trace with acceptable statistics can be obtained within a reasonable period of time. The highly accurate contrast measurements made possible by the proposed spectrometer designs are important for establishing the definition of single isolated attosecond pulses.

Acknowledgments

The work is funded by the National Science Foundation under grant number 1068604 and Army Research Office.

References

[1] E. Goulielmakis, M. Schultze, M. Hofstetter, V.S. Yakovlev, J. Gagnon, M. Uiberacker, A.L. Aquila, E.M. Gullikson, D.T. Attwood, R. Kienberger, F. Krausz, U. Kleineberg, Science 320 (2008) 1614.
[2] G. Sansone, E. Benedetti, F. Calegari, C. Vozzi, L. Avaldi, R. Flammini, L. Poletto, P. Villoresi, C. Altucci, R. Velotta, S. Stagira, S. De Silvestri, M. Nisoli, Science 314 (2006) 443.
[3] Z. Chang, Phys. Rev. A 76 (2007) 051403.
[4] Y. Mairesse, F. Quéré, Phys. Rev. A 71 (2005) 011401.
[5] M. Chini, H. Wang, S.D. Khan, S. Chen, Z. Chang, Appl. Phys. L 94 (2009) 161112.
[6] M. He Wang, S.D. Chini, S. Khan, S. Chen, X. Gilbertson, H. Feng, Z. Mashiko, Chang, J. Phys. B: At. Mol. Opt. Phys. 42 (2009) 134007.
[7] X. Feng, S. Gilbertson, S.D. Khan, M. Chini, Y. Wu, K. Carnes, Z. Chang, Opt. Express 18 (2010) 1317.
[8] J. Gagnon, V.S. Yakovlev, Opt. Express 17 (2009) 17678.
[9] S. Zhong, X. He, P. Ye, M. Zhan, H. Teng, Z. Wei, Opt. Express 21 (2013) 17498.
[10] K. Zhao, Q. Zhang, M. Chini, Y. Wu, X. Wang, Z. Chang, Opt. Lett. 37 (2012) 3891.
[11] P. Kruit, F.H. Read, J. Phys. E 16 (1983) 313.
[12] T. Tsuboi, E.Y. Xu, Y.K. Bae, K.T. Gillen, Rev. Sci. Instrum. 59 (1988) 8.
[13] F. Buchner, A. Lubcke, N. Heine, T. Schultz, Rev. Sci. Instrum. 81 (2010) 113107.

[14] K. Zhao, Q. Zhang, M. Chini, Z. Chang, in: K. Yamanouchi, K. Midorikawa (Eds.), Multiphoton Processes and Attosecond Physics, Springer-Verlag, Berlin, Germany, 2012.
[15] Simion 8.07, Scientific Instrument Service (SIS).
[16] D. Kennedy, S. Manson, Phys. Rev. A 5 (1972) 227.
[17] Q. Zhang, K. Zhao, Z. Chang, Rev. Sci. Instrum. 81 (2010) 073112.
[18] A. Kothe, J. Metje, M. Wilke, A. Moguilevski, N. Engel, Rev. Sci. Instrum. 84 (2013) 023106.
[19] M. Chini, S. Gilbertson, S.D. Khan, Z. Chang, Opt. Express 18 (2010) 13006.